NAVAL POSTGRADUATE SCHOOL
Monterey, California

THESIS

Cool-down Problem of a Solid Propellant Rocket Motor Incorporating Dewetting

by

Donald Albert Wellmann

Thesis Advisor: G. H. Lindsey

June 1972

50

Unclassified
Security Classification

DOCUMENT CONTROL DATA - R & D

(Security classification of title, body of abstract and indexing annotation must be entered when the overall report is classified)

1. ORIGINATING ACTIVITY (Corporate author)	2a. REPORT SECURITY CLASSIFICATION
Naval Postgraduate School Monterey, California 93940	Unclassified
	2b. GROUP

3. REPORT TITLE

Cool-down Problem of a Solid Propellant Rocket Motor Incorporating Dewetting

4. DESCRIPTIVE NOTES (Type of report and inclusive dates)

Degree of Aeronautical Engineer; June 1972

5. AUTHOR(S) (First name, middle initial, last name)

Donald Albert Wellmann

6. REPORT DATE	7a. TOTAL NO. OF PAGES	7b. NO. OF REFS
June 1972	51	8

8a. CONTRACT OR GRANT NO.	9a. ORIGINATOR'S REPORT NUMBER(S)
b. PROJECT NO.	
c.	9b. OTHER REPORT NO(S) (Any other numbers that may be assigned this report)
d.	

10. DISTRIBUTION STATEMENT

Approved for public release: distribution unlimited.

11. SUPPLEMENTARY NOTES	12. SPONSORING MILITARY ACTIVITY
	Naval Postgraduate School Monterey, California 93940

13. ABSTRACT

This thesis undertook a macroscopic, theoretical analysis of a long, circular, solid propellant, rocket motor undergoing thermal loading. It was shown that classical plasticity's von Mises yield condition adequately described dewetting of solid propellant which was modeled to have linear strain hardening characteristics. The mechanical properties of the propellant permitted a closed-form solution for the stresses and the strains resulting from cooling the motor from 160°F to -60°F.

DD FORM 1 NOV 68 1473 (PAGE 1)
S/N 0101-807-6811

Unclassified
Security Classification

A-31408

14 KEY WORDS	LINK A		LINK B		LINK C	
	ROLE	WT	ROLE	WT	ROLE	WT
Dewetting						
Thick-walled Cylinder						
Stress						
Strain						
Sound Propellant						
Rocket Motor						
Thermal Load						

Cool-down Problem of a Solid Propellant Rocket Motor Incorporating Dewetting

by

Donald Albert Wellmann
Lieutenant, United States Navy
B.S., United States Naval Academy, 1964
M.S., Naval Postgraduate School, 1971

Submitted in partial fulfillment of the requirements for the degree of

AERONAUTICAL ENGINEER

from the

NAVAL POSTGRADUATE SCHOOL
June 1972

Author D. Wellmann

Approved by: G. J. Lindsey
Thesis Advisor

E. A. Love
Chairman, Department of Aeronautics

Academic Dean

TABLE OF CONTENTS

I. INTRODUCTION

The problem analyzed in this thesis was that of a long, cylindrical, solid propellant rocket motor (see Figure 1) containing a circular bore and with a thin steel case bonded to its outer radius. The motor was thermally loaded by cooling it from 160°F to -60°F, which represented the extremes that might realistically be expected during its lifetime, from cure at the upper temperature to storage at the lower one. The cool-down rate was assumed to be slow enough to maintain equilibrium conditions throughout the propellant; i. e., temperature did not vary with radius. The stresses in the motor resulted from the difference in the coefficients of thermal expansion between the case and the propellant. Because the propellant had the higher of the two coefficients, it tended to contract more than the case; thus an applied load was induced at the outer boundary of the propellant.

The propellant was considered to be an isotropic, solid material; although in reality it was a composite of solid oxidizer particles imbedded in and bonded to a carbon fuel matrix. After an initial linear region, nonlinear stress-strain behavior under loading resulted from the progressive failure of these bonds at the interfaces between the fuel matrix and the oxidizer particles. Voids or vacuoles were thus created throughout the material, and their volume increased with further loading. This phenomenon is called dewetting.

Dewetting causes nonlinear material behavior and has many similarities with yielding in classical plasticity theory, as was pointed out

by Lindsey and co-workers, (4) who developed an isotropic theory for dewettable solids. In it, the strain increment was decomposed into an elastic component and a dewetted component.

$$d\varepsilon_{ij} = d\varepsilon^{e}_{ij} + d\varepsilon'_{ij} \qquad (1)$$

They further developed from Drucker's postulate that the dewetted strain increment was normal to the dewetting surface.

$$d\varepsilon'_{ij} = \lambda \frac{\partial f(\sigma_{ij}, \varepsilon_{ij})}{\partial \sigma_{ij}} \qquad (2)$$

where f=o describes the dewetting surface. From this theory, Wood (7) showed that the general form of f was

$$f = \begin{cases} J_2 - B & \text{for } I_1 \leq 0 \\ J_2 + AI_1^2 - B & \text{for } I_1 > 0 \end{cases} \qquad (3)$$

where J_2 was the second deviatoric stress invariant, I_1 was the first stress invariant, and A and B were mechanical properties. Wood experimentally measured these parameters for a PBAN propellant and found that A = -0.0026 and B = 180.

Lindsey and Wood (4) described the dewetting surface as a circular cylinder about the hydrostatic axis in principle stress space. The positive end of this cylinder was capped by a body of revolution (see Figure 2). Using a space defined by an axis system consisting of I_1^2, which was coincident with the hydrostatic axis and J_2 which was perpendicular to the hydrostatic axis, Wood's dewetting criterion became

secting straight lines with an extremely small negative slope of -0.0026 and an intersection with the J_2 axis of 180 , as shown in Figure 3. Taking the elastic propellant properties of Wood's material and the elastic solution for an encased cylinder subjected to thermal cooldown, the intersection between the thermally induced stress field and the dewetting surface was determined by calculating the ratio of J_2 and

and I_1^2, and finding its intersection with the dewetting surface. (See Figure 1) It was found that only 1 1/3% error resulted in assuming the dewetted surface was a cylinder for the thermal problem. This was quite acceptable, especially in view of the great mathematical simplification which resulted. Thus, Wood's dewetting criterion for this problem was approximated to be

$$J_2 \doteq B(T) \tag{4}$$

where for the thermal problem, B is a function of temperature. It was observed that this dewetting criterion was identical to the von Mises yield criterion of classical plasticity.

The goal of this thesis, then was to perform a stress and strain analysis using Wood's dewetting criterion as simplified accounting for the nonlinear behavior caused by dewetting, on a long, circular, solid propellant rocket motor.

Prior theory had considered propellant to be completely elastic; however, the phenomenon of dewetting was expected to occur at the inner bore initially and to expand outward as loading was increased. After yielding occurs in either dewetting or plasticity theory, the linear stress-strain law is no longer valid and must be replaced by a flow rule. Both theories insist upon a similar form of the flow rule and for the dewetting surface of equation (4), the flow law of equation (2) becomes

$$d\varepsilon'_{ij} = \lambda S_{ij} \tag{5}$$

where $d\varepsilon'_{ij}$ is the increment of dewetted strain, S_{ij} is the deviatoric stress component, and λ is a scalar incorporating the loading history. Mendelson (5) shows how λ can be written in terms of σ_e an equivalent stress, and $d\varepsilon_p$ an equivalent dewetting strain increment:

$$\lambda = \frac{3}{2}\frac{d\varepsilon_p}{\sigma_e} \tag{6}$$

In this analysis both the dewetting function and the propellant's mechanical properties (except for Poisson ratio which was assumed constant) were functions of temperature. These properties were determined experimentally for a PBAN propellant manufactured by United Technology Center, Sunnyvale, California. Thus in the solution as the temperature loading was changed, it was possible to account for variable dewetting requirements as well as variable stress-strain relationships.

II. BACKGROUND

Because of the close analogy between dewetting and plasticity, the pertinent literature of plasticity was searched for solutions to cylinder problems. It was found that the subject of partially plastic, thick-walled tubes received much attention from many authors during the late forties and the fifties. In general, the vast majority of the work dealt with internally pressurized cylinders, which were then of current interest and were more amenable to solution than those problems which deal with thermal loading.

In 1957, Steele (6) made a review of several theories for partially plastic thick-walled tubes. He stated:

> "The mathematician's approach to any problem under consideration is fundamentally different from that of the engineer. The former is interested in an accurate knowledge of the stresses and strains in terms of the applied load or loads for all points in an idealized body. In general, the engineer seeks an estimation of the variation of factors with applied loads, which are of significance only in the functional design of the part.... In the case of the thick-walled cylinder, interest lies in the deflections of the bore and the outer surface for specific internal pressures."

As an example, Hill, Lee and Tupper (2), in a rigorous work, showed that Nadai's approximate solution for the axial stress was in error by sixty percent, although the deflections at the bore and outer surface correlated closely. Rigorous solutions such as Hill's, Lee's and Tupper's, did not yield a closed form solution; and, although mathematically correct, they were so complicated that their usefulness to the engineer was minimal.

A general outline of the relationships required by the thick-walled cylinder problem is given below. These are required for any mode of loading, and apply to elastic, plastic, or dewetting theories equally.

(1) Radial Equilibrium

(2) Strain Compatability

(3) Stress-strain Relation

(4) Continuity of radial stresses and displacements across the yield surface

(5) Boundary Conditions

(6) Compressibility

(7) Yield Criteria

(8) Yield zone stress-strain relations

The boundary conditions are fixed by the geometry and the physical environment. It was assumed that at the inner bore the radial stress was zero and that the outer surface had an induced pressure caused by the restraining effect that the case applied to the propellant as the motor was cooled. Plane strain was the assumed end condition.

For mathematical simplicity in many plasticity solutions, the material has been assumed to have the same compressibility characteristics in the yielded region as in the elastic region. Furthermore, the material has been taken to be incompressible, which for metals can introduce considerable error. However, this assumption is quite valid when dealing with solid propellant, as Wood's experimental evidence has shown. Thus, it was assumed that the material was incompressible in both the dewetted and the undewetted regions. This gave considerable mathematical simplification in that Poisson's ratio, ν, was assumed to be a constant and equal to one half and that the sum of the dewetted strain increments was equal to zero.

$$d\varepsilon_r' + d\varepsilon_\theta' + d\varepsilon_z' = 0 \qquad (7)$$

This assumption permitted the simplification of the yield criterion and the stress-strain laws to useable forms.

Two yield criteria were frequently encountered. The von Mises, where

$$J_2 = \frac{\sigma_0^2}{3} \qquad (8)$$

and the Tresca yield condition, in which

$$|\sigma_1 - \sigma_3| = \sigma_0 \qquad (9)$$

The Tresca condition offered great mathematical simplicity for the cylinder problem facilitating solutions that were otherwise out of reach, provided that the relative magnitudes of the three principle stresses were known a priori. It was shown that in this problem, the axial stress was the middle stress, thus there was no need to calculate it. Additionally, its contribution to plastic yielding was zero.

On the other hand, the von Mises criterion required no prior knowledge of the stresses, but it yielded nonlinear differential equations. Due to the fact that investigators have demonstrated experimentally that the von Mises criterion provides a closer correlation with a description of yield surface than the Tresca condition, solutions have been sought and obtained for the pressure problem using the von Mises criterion. The thermal problem, however, was more difficult in that a thermal term was added to the stress-strain equation. The addition prevented a simple closed form solution using the von Mises criterion; however, it had no effect on the Tresca condition. Consequently, the Tresca condition, even though less accurate, was frequently chosen

over the von Mises criterion. Recall, though, that from dewetting theory Wood found the dewetting criterion to be of the von Mises form. It was therefore desired to obtain a solution using the von Mises surface.

There are two plastic flow rules that have been used exclusively the Prandtl Reuss and the Hencky:

Prandtl-Reuss

$$\begin{aligned} d\varepsilon'_r &= \frac{d\varepsilon_p}{\sigma_e}\left\{\sigma_r - \tfrac{1}{2}(\sigma_\theta + \sigma_z)\right\} \\ d\varepsilon'_\theta &= \frac{d\varepsilon_p}{\sigma_e}\left\{\sigma_\theta - \tfrac{1}{2}(\sigma_r + \sigma_z)\right\} \\ d\varepsilon'_z &= \frac{d\varepsilon_p}{\sigma_e}\left\{\sigma_z - \tfrac{1}{2}(\sigma_r + \sigma_\theta)\right\} \end{aligned} \qquad (10)$$

where $d\varepsilon_p$ is the equivalent plastic strain and σ_e the equivalent stress.

Hencky

$$\begin{aligned} \varepsilon'_r &= \frac{\varepsilon_p}{\sigma_e}\left\{\sigma_r - \tfrac{1}{2}(\sigma_\theta + \sigma_z)\right\} \\ \varepsilon'_\theta &= \frac{\varepsilon_p}{\sigma_e}\left\{\sigma_\theta - \tfrac{1}{2}(\sigma_r + \sigma_z)\right\} \\ \varepsilon'_z &= \frac{\varepsilon_p}{\sigma_e}\left\{\sigma_z - \tfrac{1}{2}(\sigma_r + \sigma_\theta)\right\} \end{aligned} \qquad (11)$$

The Prandtl-Reuss equations deal with incremental theory where an increment of plastic strain is so small that it can be considered linear. The total plastic strain is achieved by integration. An expansion of equation (5) for dewetting materials shows it to be identical to the Prandtl-Reuss equations.

Hencky postulated that the total plastic strain would have the same type of relationship as the incremental such that the present state of plastic strain was independent of its loading path. This is not true in general, and the Hencky relationships have fallen into disuse. However, under special circumstances of linear strain hardening and a monotomically increasing load, the two flow rules coincide (5).

Steele presented a summary of the combinations of these parameters that have been tried by different researchers. It is repeated here in Table I. Note that most of the solutions required numerical analysis. Any numerical solution necessitates a loss of generality and makes a parameter study more costly and difficult. Thus a closed form solution was desired. By making simplifying approximations which were the result of either the special geometry assumed or the unique mechanical properties of solid propellant, it was possible to obtain a closed form solution to the thermal problem using a von Mises dewetting surface.

III. THEORETICAL ANALYSIS

Within the above mentioned framework and background, the theoretical analysis was undertaken. Figure 2 describes the geometry of the problem, and the governing equations are given below.

Equilibrium

$$\frac{d\sigma_r}{dr} \quad \frac{\sigma_r - \sigma_\theta}{r} = 0 \tag{12}$$

Strain Compatability

$$\frac{d\varepsilon_\theta}{dr} \quad \frac{\varepsilon_\theta - \varepsilon_z}{r} = 0 \tag{13}$$

Stress-Strain

$$\begin{aligned} \varepsilon_r &= \frac{1}{E}\{\sigma_r - \nu(\sigma_\theta + \sigma_z)\} + \alpha T + \varepsilon'_r \\ \varepsilon_\theta &= \frac{1}{E}\{\sigma_\theta - \nu(\sigma_r + \sigma_z)\} + \alpha T + \varepsilon'_\theta \\ \varepsilon_z &= \frac{1}{E}\{\sigma_z - \nu(\sigma_r + \sigma_\theta)\} + \alpha T + \varepsilon'_z \end{aligned} \tag{14}$$

where $\varepsilon'_{r,\theta,z}$ are the dewetted strain components.

The problem was well structured in that there were sufficient equations to accommodate the unknowns; thus, a unique solution could be derived. By applying the plane strain assumption and the incompressibility condition of the dewetted zone, the last of equations (14) was solved for the axial stress

$$\sigma_z = 1/2(\sigma_r + \sigma_\theta) - E\alpha T + E(\varepsilon'_\theta + \varepsilon'_r) \tag{15}$$

Using this definition of the axial stress, the first two stress-strain relations (equations (14) were substituted into the strain compatability equation (equation (13)) yielding a differential equation in terms of σ_θ and σ_r. The tangential stress, σ_θ, was eliminated through the use of the equilibrium equation (equation (12)), yielding

$$\frac{d}{dr}\left\{\frac{1}{E}\left[\tfrac{1}{2}\left(\sigma_r + r\frac{d\sigma_r}{dr}\right) - \tfrac{1}{2}\sigma_r\right] - \frac{1}{3}\left(\varepsilon_r' - \varepsilon_\theta'\right)\right\} + \frac{1}{E}\frac{d\sigma_r}{dr} - \frac{2}{3}\left(\frac{\varepsilon_r' - \varepsilon_\theta'}{r}\right) = 0 \tag{16}$$

Integrating this equation twice yielded an expression for the radial stress.

$$\sigma_r = -\frac{EC_1}{r^2} + \frac{2E}{3}\int_a^r \frac{\varepsilon_r' - \varepsilon_\theta'}{r}\,dr - \frac{2E}{r^2}\int_a^r \alpha T r\,dr + C_2 \tag{17}$$

where C_1 and C_2 were constants of integration. Analytic integration is only possible when Poisson's ratio is one-half, which is the actual value for propellant.

The temperature distribution was assumed to be constant as previously mentioned. Consequently, the temperature integral of equation (17) was readily evaluated.

$$\sigma_r = -\frac{EC_1}{r^2} + \frac{2E}{3}\int_a^r \frac{\varepsilon_r' - \varepsilon_\theta'}{r}\,dr - E\alpha T\left(1 - \frac{a^2}{r^2}\right) + C_2 \tag{18}$$

The two constants of integration were evaluated by applying the boundary conditions:

$$\begin{aligned} &\text{at } r = a \qquad \sigma_r = 0 \\ &\text{at } r = b \qquad \sigma_r = p' \end{aligned} \tag{19}$$

where p' was the pressure at the boundary between the propellant and the case and was caused by the difference between the case's coefficient of thermal expansion and that of the propellant. See Appendix A. Application of the first boundary condition yielded

$$C_2 = \frac{E C_1}{a^2} \tag{20}$$

Applying the second boundary condition at r = b, gives

$$C_1 = \frac{b^2a^2}{E(b^2 - a^2)}\left[-p' - \frac{2E}{3}\int_a^b \frac{\varepsilon_r' - \varepsilon_\theta'}{r}\,dr + E\alpha T\left(\frac{b^2 - a^2}{b^2a^2}\right)\right] \tag{21}$$

Substituting (19) and (21) back into the expression for σ_r yielded

$$\sigma_r = \frac{b^2(r^2 - a^2)}{r^2(b^2 - a^2)}\left[-p' - \frac{2E}{3}\int_a^b \frac{\varepsilon_r' - \varepsilon_\theta'}{r}\,dr + E\alpha T\left(\frac{b^2 - a^2}{b^2a^2}\right)\right] + \frac{2E}{3}\int_a^r \frac{\varepsilon_r' - \varepsilon_\theta'}{r}\,dr - E\alpha T\left(1 - \frac{a^2}{r^2}\right) \tag{22}$$

The need was now to solve the remaining dewetted strain integrals. As mentioned above, it had been assumed that the Lindsey dewetted stress strain equations applied and that solid propellant possessed linear strain hardening characteristics. Expanding equations (5) gives

$$\begin{aligned} d\varepsilon_r' &= \frac{d\varepsilon_p}{\sigma_e}\left\{\sigma_r - \tfrac{1}{2}(\sigma_\theta+\sigma_z)\right\} \\ d\varepsilon_\theta' &= \frac{d\varepsilon_p}{\sigma_e}\left\{\sigma_\theta - \tfrac{1}{2}(\sigma_r+\sigma_z)\right\} \end{aligned} \tag{23}$$

As previously stated, for monotonically increasing loads and a linearly strain hardening material, the Prandtl-Reuss equations degenerated to the Hencky equations. Within this approximation, therefore, it was assumed that the Lindsey equations took the form of

$$\begin{aligned} \varepsilon_r' &= \frac{\varepsilon_p}{\sigma_e}\left\{\sigma_r - \tfrac{1}{2}(\sigma_\theta+\sigma_z)\right\} \\ \varepsilon_\theta' &= \frac{\varepsilon_p}{\sigma_e}\left\{\sigma_\theta - \tfrac{1}{2}(\sigma_r+\sigma_z)\right\} \end{aligned} \tag{24}$$

From those equations it is seen that

$$\varepsilon_r' - \varepsilon_\theta' = \frac{3}{2}\,\frac{\varepsilon_p}{\sigma_e}\,(\sigma_r - \sigma_\theta) \tag{25}$$

where

$$\begin{aligned} \varepsilon_p &= \frac{\sqrt{2}}{3}\left[(\varepsilon_\theta'-\varepsilon_z')^2+(\varepsilon_z'-\varepsilon_r')^2+(\varepsilon_r'-\varepsilon_\theta')^2\right]^{1/2} \\ \sigma_e &= \sqrt{3J_2} = \frac{1}{\sqrt{2}}\left[(\sigma_\theta-\sigma_z)^2+(\sigma_z-\sigma_r)^2+(\sigma_r-\sigma_\theta)^2\right]^{1/2} \end{aligned} \tag{26}$$

The axial stress, , was replaced by equation (15), and after expanding the terms and regrouping

$$\sigma_e = \sqrt{3}\,\left[(\sigma_r-\sigma_\theta)^2-\left(\frac{E\alpha T+E(\varepsilon_r'+\varepsilon_\theta')}{3}\right)^2\right]^{1/2} \tag{27}$$

An examination for order of magnitude of each term of the right side of equation (27) demonstrated that the square of the stress difference clearly dominated the entire expression. The radial and tangential stresses were of opposite sign and such size that their difference was relatively large. The low modulus of the propellant relative to that

of some other material such as steel (see Figure 13) made the $E\alpha T$ term small compared to the stress difference. Additionally, from the elastic solution, it is seen that the radial strain is negative while the tangential strain is positive. Moreover, the absolute magnitude of the radial strain is larger than that of the tangential strain; consequently the sum of the tangential and radial dewetted strain components must be negative, assuming that the direction of the dewetted strain increments are in the same direction as their elastic components. So it seems that the already small $E\alpha T$ term is reduced even more by the addition of this negative quantity. Thus, the second term inside the radial was neglected. The expression for the equivalent stress became

$$\sigma_e \doteq \sqrt{3}\,|\sigma_r - \sigma_\theta| \tag{28}$$

which simplification made possible a closed form solution without appreciable loss in accuracy. The terms neglected were estimated to constitute at most a 2% error.

Using equation (28), equation (25) reduced to

$$\varepsilon_r' - \varepsilon_\theta' = \frac{\sqrt{3}}{2}\,\varepsilon_p\,\mathrm{sgn}(\sigma_r - \sigma_\theta) \tag{29}$$

where $\mathrm{sgn}(\sigma_r - \sigma_\theta) < 0$ for the thermal problem.

The significance of assuming linear strain hardening actually meant that the stress-strain curve was approximated by two straight lines, one having the slope of E and the second having the slope of mE as shown in Figure 4. From the figure an expression for the dewetted region was found to be

$$\varepsilon_p = \frac{(1-m)(\sigma_e - \sigma_o)}{mE} \tag{30}$$

By taking equation (28) and applying the equilibrium equation (12) it is seen that

$$\sigma_e = \sqrt{3}\,\frac{r\,d\sigma_r}{dr} \tag{31}$$

Using equations (31, 30, 29) permitted direct integration of the dewetted strain integral in equation (22) such that the radial stress expression became

$$\sigma_r = \frac{m}{4m-3}\left\{-\frac{(r^2-a^2)b^2}{(b^2-a^2)r^2}\left[-p' - \frac{\sqrt{3}(1-m)}{m}\left(\sqrt{3}\,\sigma_{r_c} + \sigma_0 \ln(a/r_c)\right)\right] + \sqrt{3}\,\frac{(1-m)}{m}\,\sigma_0 \ln a/r\right\} \tag{32}$$

Two new unknown constants appeared in this equation, σr_c and r_c. The critical radius, r_c, was the radius of the boundary between the dewetted and the elastic zones, and σ_{r_c} was the radial stress at this boundary. Both of these were constant and were functions of the thermal loading only. σ_{r_c} was related to r_c by setting r equal to r_c in equation (32). After substituting for p'

$$\sigma_{r_c} = \frac{-\frac{(r_c^2-a^2)b^2}{(b^2-a^2)r_c^2}\left\{-\frac{3ET(\alpha-\alpha_c)}{2D} - \frac{\sqrt{3}(1-m)}{m}\sigma_0 \ln a/c\right\} + \frac{\sqrt{3}(1-m)}{m}\sigma_0 \ln a/c}{\frac{4m-3}{m} - \frac{(r_c^2-a^2)b^2}{(b^2-a^2)r_c^2}\left(\frac{3r_c^2}{2(b^2-r_c^2)} + \frac{3(1-m)}{m}\right)} \tag{33}$$

where p' and D came from the elastic solution. (See Appendix A.)

It was noted that at the boundary between the dewetted and undewetted zones, the radial stress must be continuous across the boundary. Further, note at that location that the dewetted condition must also be met by the stresses in both the elastic and the dewetted regions.

The yield condition, equation (1) became

$$(\sigma_r - \sigma_\theta) = 2\sqrt{B(T) - \frac{(E\alpha T)^2}{3}} \tag{34}$$

The second term under the radical was considered negligible for reasons already given. The expression for σ_r and σ_θ were taken from Appendix A. The combined loading case was used, and the radius was set equal to the critical radius ($r=r_c$), such that

$$(\sigma_r - \sigma_\theta) = \frac{\sigma_{r_c} a^2\left(-2b^2 + \frac{3b^2a^2}{D(b^2-a^2)}\right) + 3b^2a^2\frac{ET(\alpha-\alpha_c)}{D}}{r_c^2\,(b^2-a^2)} \tag{35}$$

Combining equations (34) and (35) and solving for r_c yielded

$$r_c = \left[\frac{\frac{3}{2}\frac{b^2 E T(\alpha-\alpha_c)}{\sqrt{B}} + \frac{b^3(1-\nu_c^2)}{E_c h}\left(\frac{\sigma_{r_c}}{\sqrt{B}} - 1\right)}{\frac{3}{2} - \frac{(1-\nu_c^2)bE}{E_c h}} \right]^{1/2} \qquad (36)$$

It would have been possible to solve equation (34) and (35) for σ_{r_c} in terms of an unknown r_c and to set this new expression equal to equation (33), solving for r_c directly. However, such a course of action would have resulted in a transcendental, tenth order expression and would have been of little practical value. A simpler method was to iterate with equations (36 and (33). Assume a value for σ_{r_c} (say $\sigma_{r_c} = 0$) and solve for r_c by using equation (36). This value for r_c was used in equation (33) to solve for a better value of σ_{r_c}. This process was repeated until the resulting values of r_c converged.

All unknown constants of equation (32) were known and the complete expression for the radial stress was obtained:

$$\underline{r \le r_c} \quad \sigma_r = \frac{m}{4m-3}\left\{ -\frac{(r^2-a^2)b^2}{(b^2-a^2)r^2}\left[-p' - \frac{\sqrt{3}(1-m)}{m}\left(\sqrt{3}\sigma_{r_c} + \sigma_0 \ln\frac{a}{r_c}\right)\right] + \sqrt{3}\frac{(1-m)}{m}\sigma_0 \ln\frac{a}{r} \right\} \qquad (37)$$

$$\underline{r > r_c} \quad \sigma_r = -\frac{(r^2-a^2)b^2}{(b^2-a^2)r^2}\left\{ -p' - \frac{\sqrt{3}(1-m)}{m}\left(\sqrt{3}\sigma_{r_c} + \sigma_0 \ln\frac{a}{r_c}\right)\right\} + \frac{\sqrt{3}(1-m)}{m}\left\{\sqrt{3}\sigma_{r_c} + \sigma_0 \ln\frac{a}{r_c}\right\} \qquad (38)$$

Through the application of the equilibrium equation, the tangential stress was obtained directly.

$$\underline{r \le r_c} \quad \sigma_\theta = \sigma_r - \frac{m}{4m-3}\left\{ \frac{2b^2a^2}{(b^2-a^2)r^2}\left[-p' - \sqrt{3}\frac{(1-m)}{m}\left(\sqrt{3}\sigma_{r_c} + \sigma_0 \ln\left(\frac{a}{r_c}\right)\right)\right] + \sqrt{3}\frac{(1-m)}{m}\sigma_0 \right\}$$

$$\underline{r > r_c} \quad \sigma_\theta = \sigma_r - \frac{2b^2a^2}{(b^2-a^2)r^2}\left\{ -p' - \sqrt{3}\frac{(1-m)}{m}\left(\sqrt{3}\sigma_{r_c} + \sigma_0 \ln a/r_c\right)\right\} \qquad (39)$$

The strains were obtained by application of the stress-strain equations.

$$\varepsilon_r = \frac{3}{4}\frac{(2m-1)}{m}\frac{(\sigma_r - \sigma_0)}{E} + \frac{3}{2}\alpha T - \frac{\sqrt{3}\sigma_0}{4Em} \qquad (40)$$

$$\varepsilon_\theta = \frac{3}{4}\frac{(1-2m)}{m}\frac{(\sigma_r - \sigma_\theta)}{E} + \frac{3}{2}\alpha T + \frac{\sqrt{3}\sigma_0}{4Em}$$

IV. EXPERIMENTAL RESULTS

There was a dual goal in the experimental work done. First, it was necessary to experimentally determine the constant, B(T) in equation (2), for the particular PBAN propellant used. This was accomplished by conducting uniaxial tensile tests over a range of temperatures in the gas dilatometer of United Technology Center, Sunnyvale, California. For uniaxial tension, Equation (2) reduced to:

$$B(T) = \frac{\sigma_0^2}{3} \tag{41}$$

The dilatometer (see Figures 5, 6, 7, 8) utilized the Perfect Gas Law as its basic operational principle. The specimen was mounted within a sealed chamber and pull-rods extended from either end of the sample through the ends of the chamber and attached to the cross-head of an Instron testing machine. Any change in the volume of the sample while under load resulted in a change in the chamber's pressure creating a pressure difference across a diaphram separating the test chamber from an adjoining reference cavity. A baratron pressure transducer converted this pressure difference into an electrical signal, which was fed to one pen of a two-pen X-Y plotter. The signal for the second pen came from a load cell in the cross-head of the Instron machine. The raw data thus obtained were in the form of two superimposed plots; one was the time history of the load, and the second was the time history of the dilatation. By using the constant cross-head speed and premeasuring both the cross sectional area and gage length, the data was reduced to plots of stress vs strain and dilatation vs strain. (See Figure 9)

Changes in the ambient temperature caused a problem since it affected the readings of the pressure transducer through the same Perfect Gas Law. In order to isolate the experiment from ambient temperature fluctuations and also provide a method of controlling the temperature at which the experiment was conducted, the dilatometer was enclosed in a temperature box, which possessed the capability of maintaining a preselected temperature to within a degree over the duration of the experiment. Although the ambient temperature within the temperature box was fairly constant, at subzero temperatures, heat leaked into the dilatometer probably by conduction through the push rods. A large temperature drift would develop after about one half hour and this dictated the maximum duration of any individual run.

The second goal was to experimentally determine the mechanical properties of the subject propellant as functions of temperature; namely, the uniaxial dewetting stress, σ_o , and the elastic modules, E and m. (See Figures 10, 11, 12)

The test samples were square with sides machined to approximately one half inch, and they had a gage length of approximately 2 3/4 inches. Redwood tabs were bonded to each end of the sample to make hardware attachment possible. Tests were conducted at 21°C, 3°C, -9°C, -21°C, and -52°C, with four tests being conducted at the three higher temperatures, two tests conducted at -21°C and one test conducted at -52°C. Experimental difficulties with the equipment at the subzero temperatures resulted in the reduced number of runs at the lower temperature. Experimental scatter of seven to ten percent was found in the dilatation and stress-strain curves. However, only about five percent scatter was

found among the parameters measured (i.e., E, m, and σ_o). Due to the fragile nature of solid propellant specimens, this was considered quite reasonable results.

After reducing the raw data to the stress vs strain and dilatation vs strain plots mentioned above, the problem of identifying σ_o developed. Three methods were available from the literature: (1) interpreting the stress which corresponds to the lift-off point of the dilatation curve as σ_o. This method provided results which were quite repeatable; however, the stress strain curve did not depart from its initial linear relationship at this point. (2) The dilatation curves eventually assume a constant slope. Physically the total amount of solid material which could dewet had dewetted at this point and further dilatation resulted only from increasing the size of previously formed voids. The stress corresponding to the extrapolation of this constant slope line back to the zero stress point (pt. B) of Figure 13 would be considred as the yield stress, σ_o. This could be physically interpreted as assuming that no dewetting occurred until the yield stress was reached; then all the dewetting occurred simultaneously. This was tantamount to assuming that the propellant was perfectly plastic. However, at the lower temperatures, specimen failure resulted before such a linear portion to the dilatation curve was reached. (3) The third method was to take the stress at the point where the stress-strain curve initially departed from a linear relationship. This method reflected the linear-strain hardening assumption, and provided consistent reproduceable results from sample to sample. It neglected the dilatation curve altogether. This last method was adopted primarily because it met the condition

of the linear strain hardening assumption. A comparison of these three methods was given in Table II, where it is seen that methods (2) and (3) yield similar results.

The test speeds were chosen as slow as possible, yet fracture had to be reached within the time limit mentioned above. At the lower temperatures, it was assumed that the speeds used maintained the specimens in equilibrium and that the load did not produce viscoelastic effects.

In summary, the yield stress, σ_o, was taken as the stress at which the average stress strain curve first departed from linearity for all runs at any one temperature. The modulus, E, was the average of the elastic slopes of the stress-strain diagrams for any given temperature. The strain hardening exponent, m, was the ratio of the slope for the least squares straight line fit of the non-linear portion of the stress strain curve, to the initial modulus.

V. RESULTS AND CONCLUSIONS

A. RESULTS

In order to compare the results predicted by dewetting theory with those obtained from linear elastic theory, a sample problem was worked. A PBAN propellant of current interest was used, and its mechanical properties were experimentally determined, (Figures 11, 12). The other required parameters were taken from Appendix II of Reference (4).

For the propellant: $\nu = 1/2$ $\alpha = 2.21 \times 10^{-5}$ in./in./°F

For the steel case: $\nu_c = 1/3$ $\alpha_c = .65 \times 10^{-5}$ in./inc./°F

$E_c = 3 \times 10^7$ psi

Geometrical parameters: a= 3in. b= 12in. h=0.015in.

The rocket motor was cooled from 160°F to -60°F, and both elastic and dewetted stress-strain analyses were made. Linear strain hardening was assumed which enabled calculations to be performed in two steps: one elastic step and one dewetted step. The temperature was not incrementally stepped down. Equations (32) and (36) were iterated in order to find the critical radius, r_c, and the interface stress, σ_{r_c}. These results were plotted in Figure (14). It was interesting to note that the growth of the yield surface was linear with temperature. Furthermore, dewetting did not begin until the temperature had been decreased to 10°F, and at the lower temperature limit the yield surface had penetrated to a radius of only 9 1/2 inches. The interface pressure also increased linearly as the temperature was lowered reflecting the influence of temperature on both the yield criterion and the propellant's mechanical properties.

The greatest effect of dewetting was upon the tangential and radial stresses. (Figures 15, 16) The tangential stress at the bore, for both the elastic and the dewetting theories, was plotted against temperature. It was seen that dewetting substantially relieved the stress. The radial stress was plotted across the motor's thickness for a characteristic temperature of -8.0°F. Again it was shown that stress was relieved within the dewetted region. The radial stress then approached the elastic solution as one moved deeper into the undewetted elastic material and away from the critical radius. However, a pronounced effect of the induced pressure at the inner radius of the undewetted region was still evident.

Initially, the behavior of the tangential strain at the bore was quite surprising. (See Figure (17)) It had been anticipated that this strain would have been negative and would have increased in magnitude as the temperature was lowered. However upon looking at the elastic tangential strain equation (A-1), one sees that it consists of two terms. The first term represents the mechanical strain imposed by the case upon the propellant. It is positive and dominates the second term, the thermal strain, which is negative in the cool-down problem. However, as the temperature is lowered the mechanical properties of the propellant change significantly, and the negative ΔT term grows in relative magnitude, actually forcing the total strain to decrease. Thus, it was observed that the maximum strain occurred at about 40°F instead of at the lower temperature extremum.

B. CONCLUSIONS

A point worthy of note is the curve fit of the m curve coefficient of linear strain hardening in figure 12. Equipment limitations at the subzero temperatures, which restricted multiple runs decreased confidence in the values of m. Consequently, the specific mechanical properties measured at -5.8°F and -60°F were used to calculate the bore hoop strain at those two temperatures, and they appear on the plot in Figure 14 which uses the curve fit for m. It was concluded that a curve fit which averaged these values provided, a smoother extension of the elastic solution than a curve which connected each data point. Further tests would prove useful to more definitely fix the m curve.

From a comparison of the elastic and the dewetting solutions for both stresses and strains it was concluded that dewetting has little effect on the strains. In an incompressible material the strains are fixed by geometrical constraints and not by mechanical properties. However, stresses are tied to the mechanical properties and thus are greatly affected by dewetting.

It was further concluded that a thermo-dewetting solution could be obtained in a relatively simple form and that better results for stress would be obtained by using dewetting theory vice elastic theory.

TABLE I

COMPARISON OF SOLUTIONS FOR THE THICK-WALLED PLASTIC CYLINDER PROBLEM

Author	Plastic Stress strain law	Compressibility: Plastic domain	Compressibility: Elastic domain	Flow condition	Axial boundary	Type of solution
Hill, Lee, and Tupper (1)	Prandtl-Reuss	Comp	Comp	Tresca	$\epsilon_z = 0$	Numerical
Hill, Lee, and Tupper (15)	Prandtl-Reuss	Comp	Comp	Tresca	Closed ends	Numerical
MacGregor, Coffin, and Fisher (12)	Hencky	Comp	Comp	von Mises	Open ends	Numerical
Sokolovsky (16)	Hencky	Comp	Comp	von Mises	$\epsilon_z = 0$	Numerical
Sokolovsky (16)	Hencky	Comp	Comp	von Mises[a]	$\epsilon_z = 0$	Numerical
Sokolovsky (16)	Hencky	Incomp	Comp	von Mises	$\epsilon_z = 0$	Closed form
Sokolovsky (16)	Hencky	Incomp	Comp	von Mises[a]	$\epsilon_z = 0$	Numerical
Hodge and White (10)	Prandtl-Reuss	Comp	Comp	von Mises	$\epsilon_z = 0$	Numerical
Hodge and White (10)	Hencky	Comp	Comp	von Mises	$\epsilon_z = 0$	Numerical
Allen and Sopwith (11)	Hencky	Comp	Comp	Tresca	Either $\epsilon_z = 0$, or closed ends, or open ends	Closed form
Cook (17)	Hencky	Incomp	Comp	Tresca with upper and lower yield	Closed ends	Closed form[b]
Nadai (2)	Hencky	Incomp	Com	von Mises	$\epsilon_z = 0$	Closed form
Steele (13)	Hencky	Incomp	Comp	Tresca	Either $\epsilon_z = 0$, or closed ends, or open ends	Closed form
Steele (theory of this paper)	Hencky	Incomp	Comp or Incomp	Tresca	Either $\epsilon_z = 0$, or closed ends, or open ends	Closed form

[a] Inclusion of strain-hardening; nonasterisked solutions assume material to flow according to function defining theory of failure.

[b] Solution dependent on experimental measurements which Cook made on closed-ended cylinders.

TABLE II

TABULATION OF EXPERIMENTAL DATA

Temp	σ_o	E	m
21°	94	806	.417
3.5	118	983	.545
-9	137	1600	.49
-21	159	8840	.369
-52.5	231	23100	.539

TABLE III.

COMPARISON OF METHODS OF READING
TENSILE YIELD STRESS

TEMPERATURE (°C)	σ_o (psi) I	II	III
22°	46	84.5	94
3.5	72.5	107	118
-9	105	*	137
-21	137	*	159
-52.5	201	*	231

*Dilatation Curve did not reach constant slope.

I. σ_o was stress corresponding to the lift off point of the Dilatation Curve.

II. σ_o was stress corresponding to extrapolation of of the constant Dilatation Curve back to the strain axis.

III. σ_o was stress at which stress-strain curve initially departed from a linear relationship.

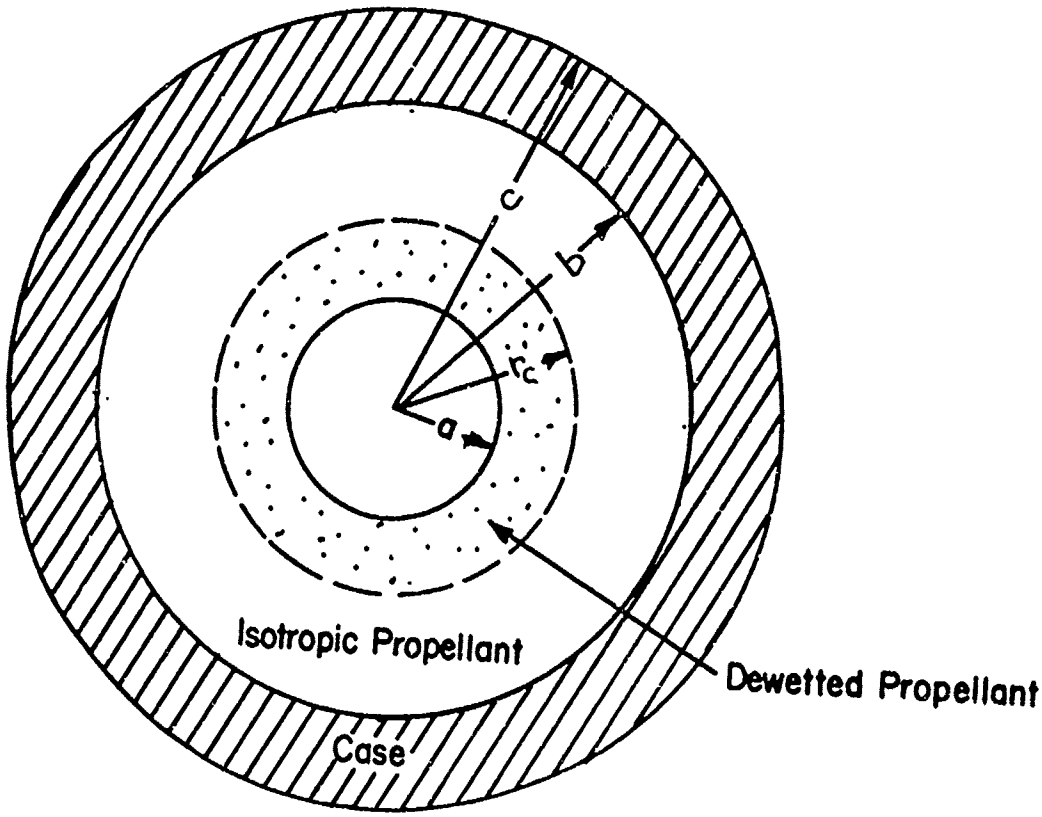

Rocket Motor Geometry

Figure 1.

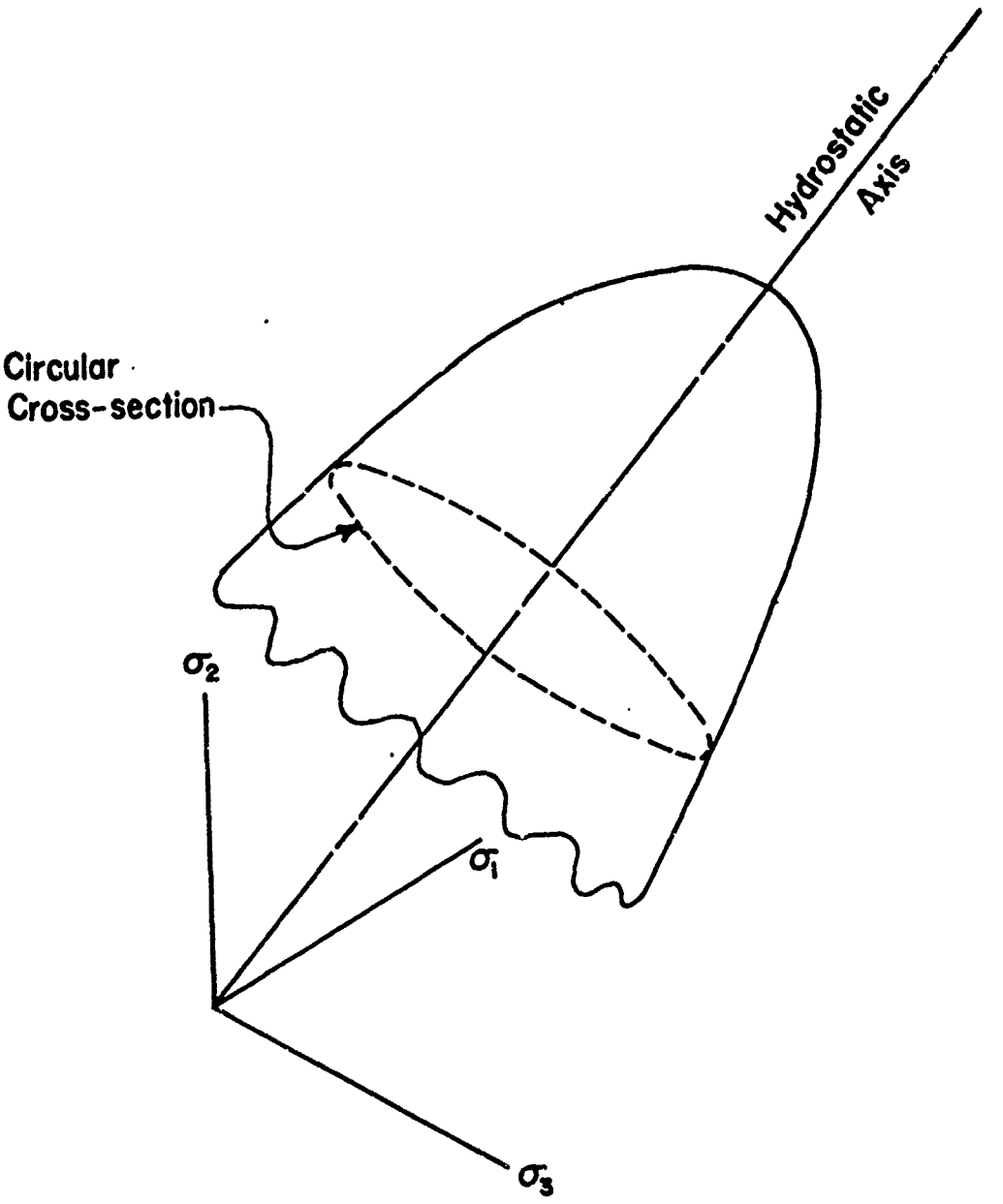

Dewetted Yield Surface in Principle Stress Space

Figure 2.

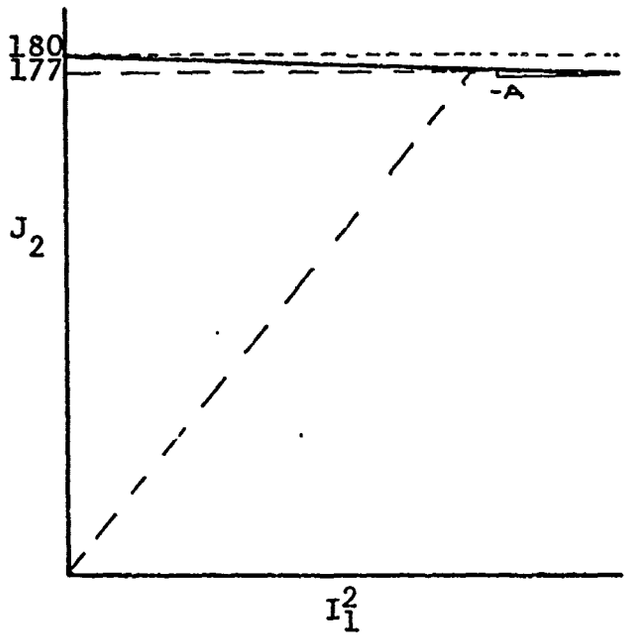

Intersection of Thermal Stress Load
with Dewetting Surface

Figure 3.

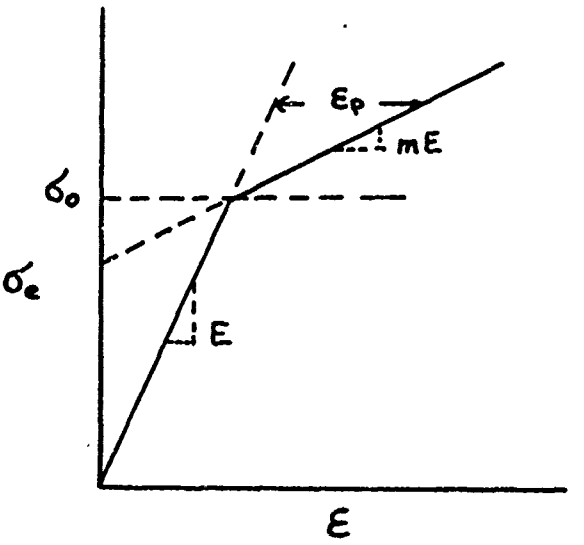

Linear Strain Hardening

Figure 4.

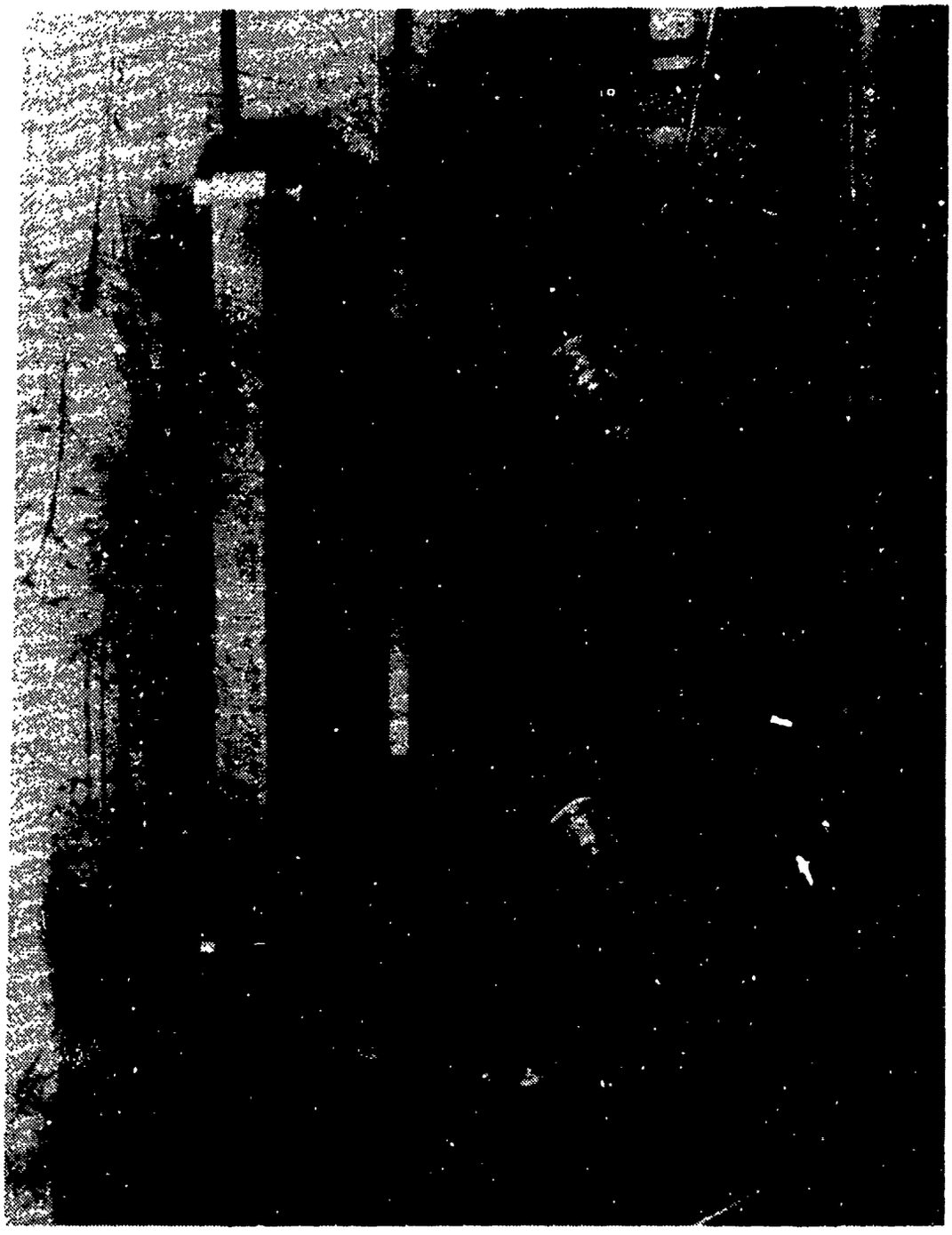

FIGURE 5

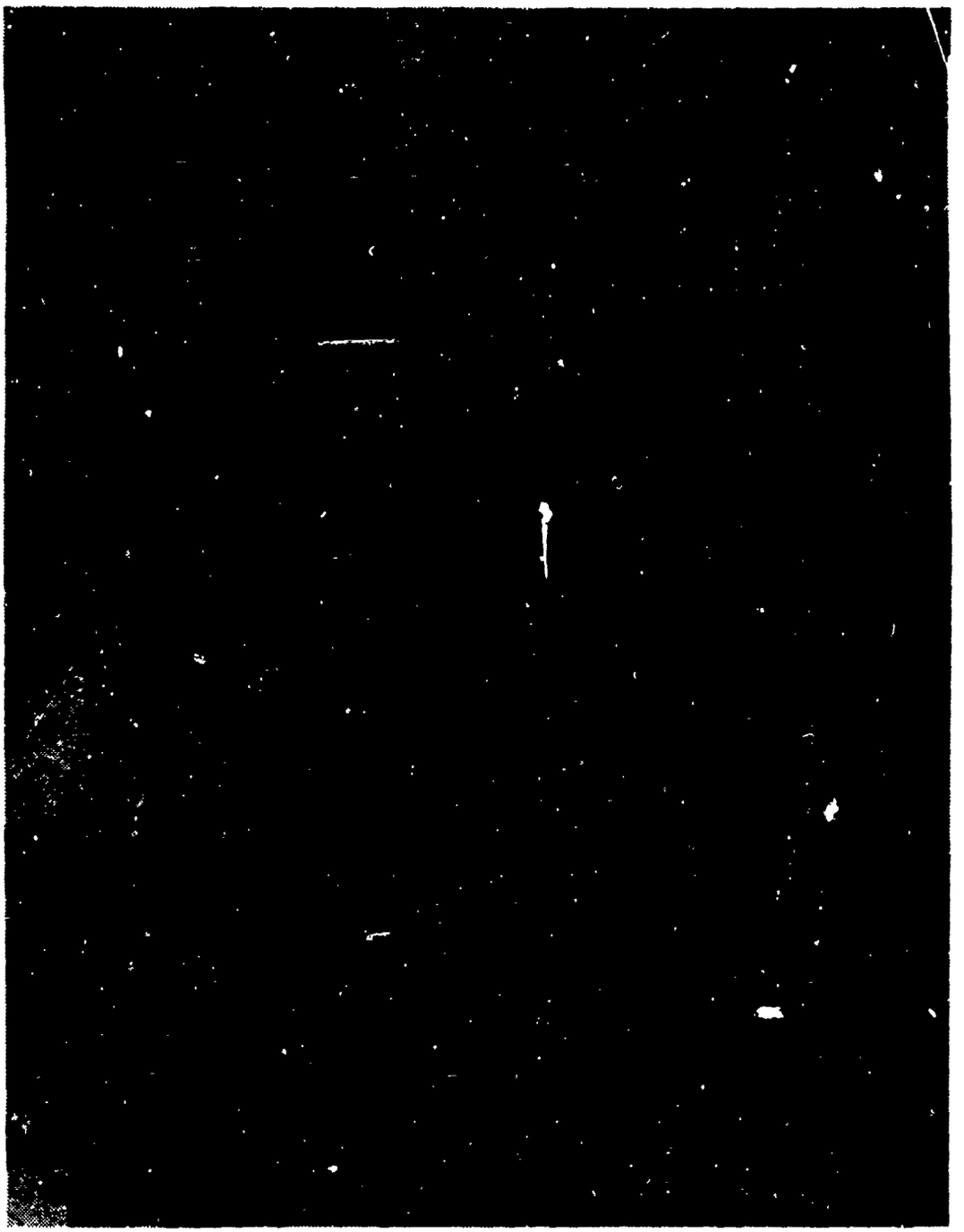

FIGURE 6

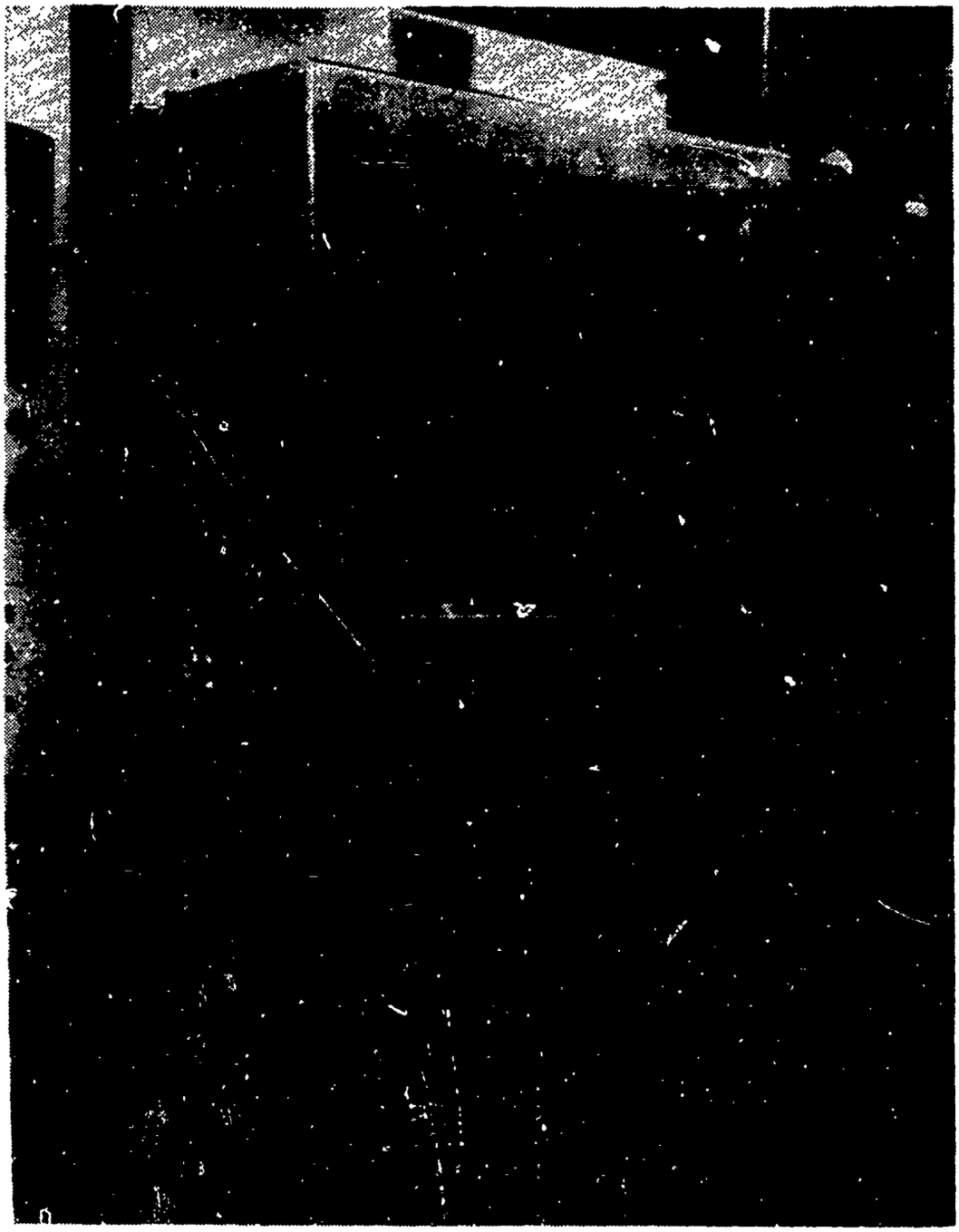

FIGURE 7

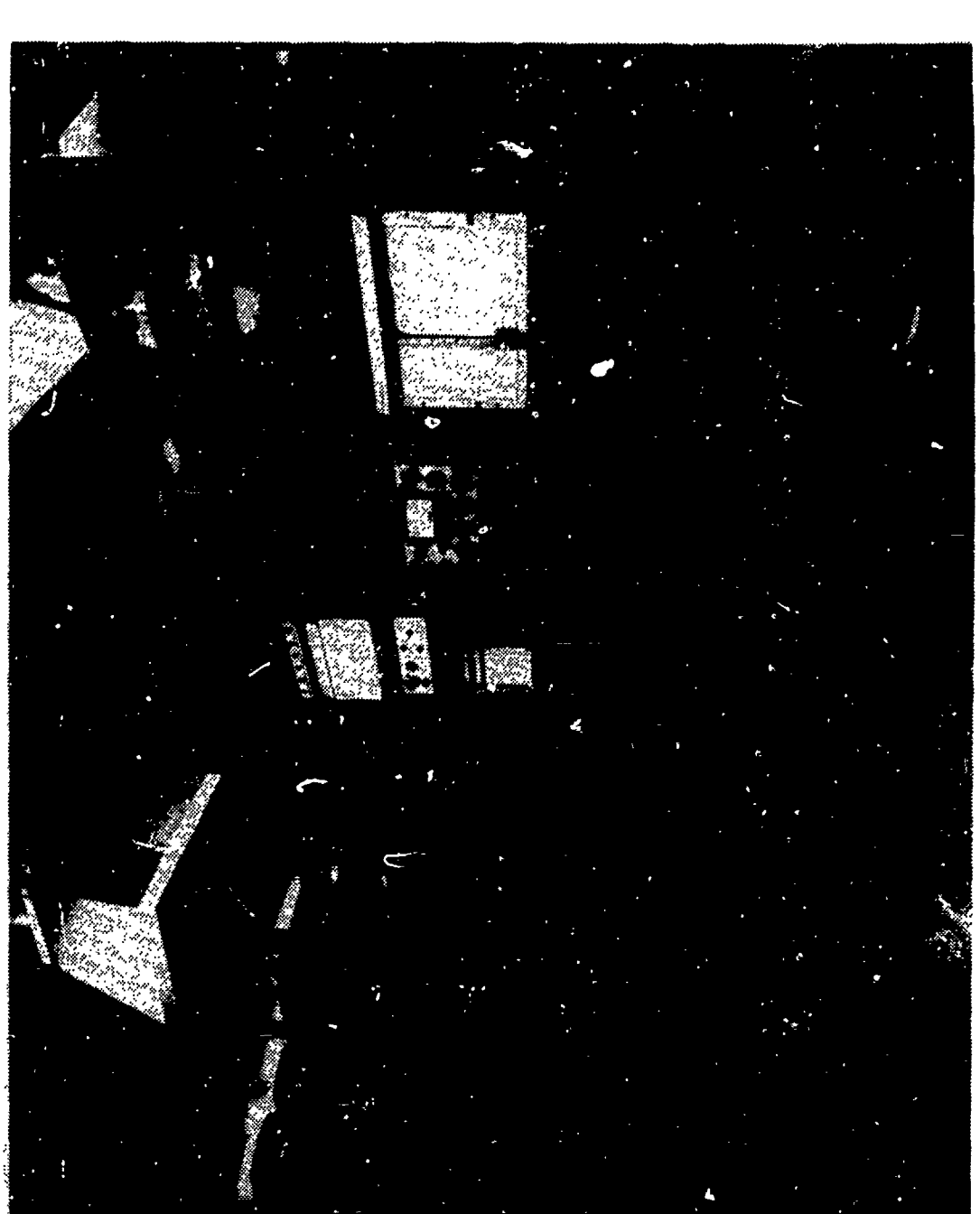

FIGURE 8

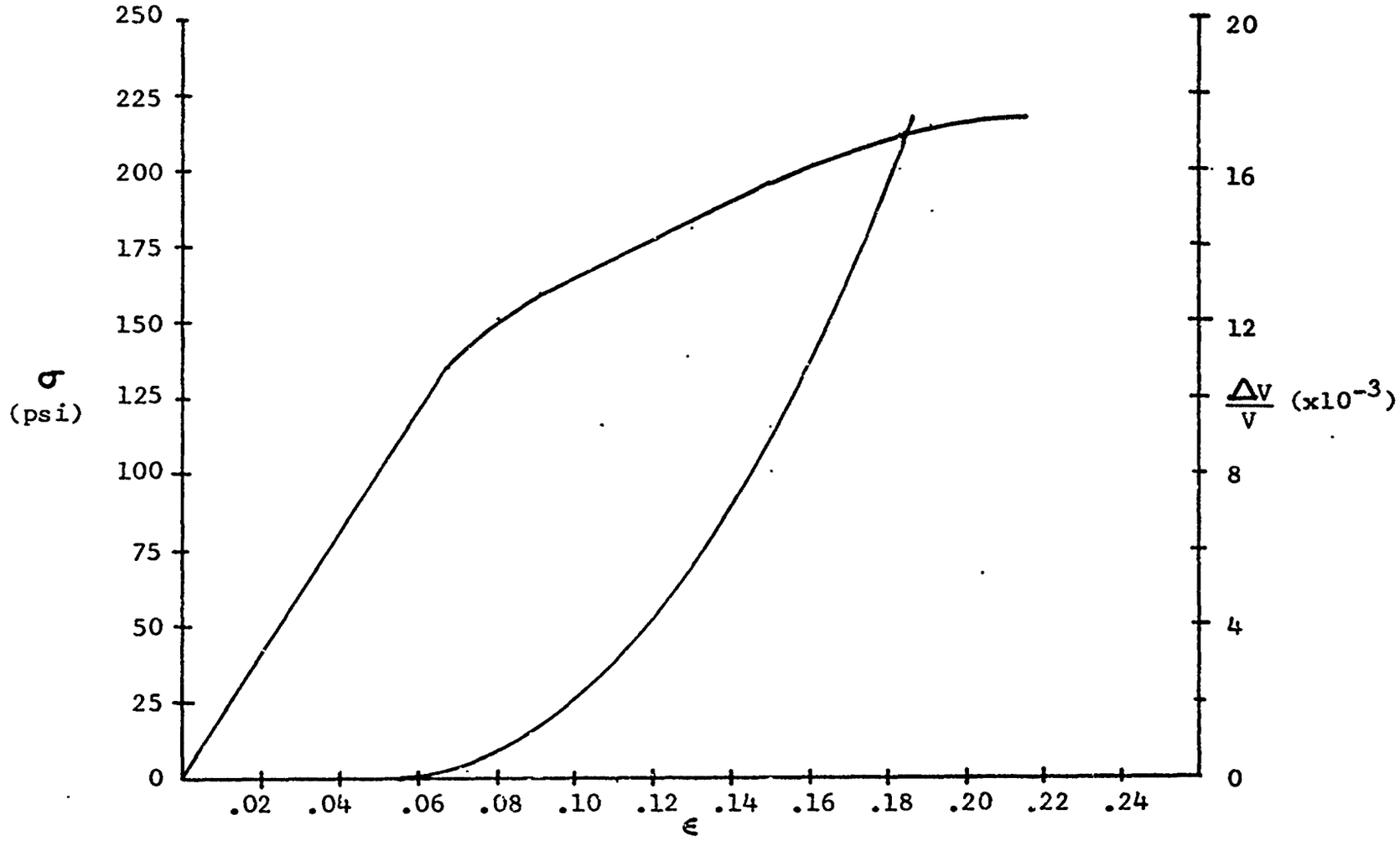

UNIAXIAL TENSILE STRESS VS STRAIN/DILATATION VS STRAIN
(Temp = 20°F)

Figure 9

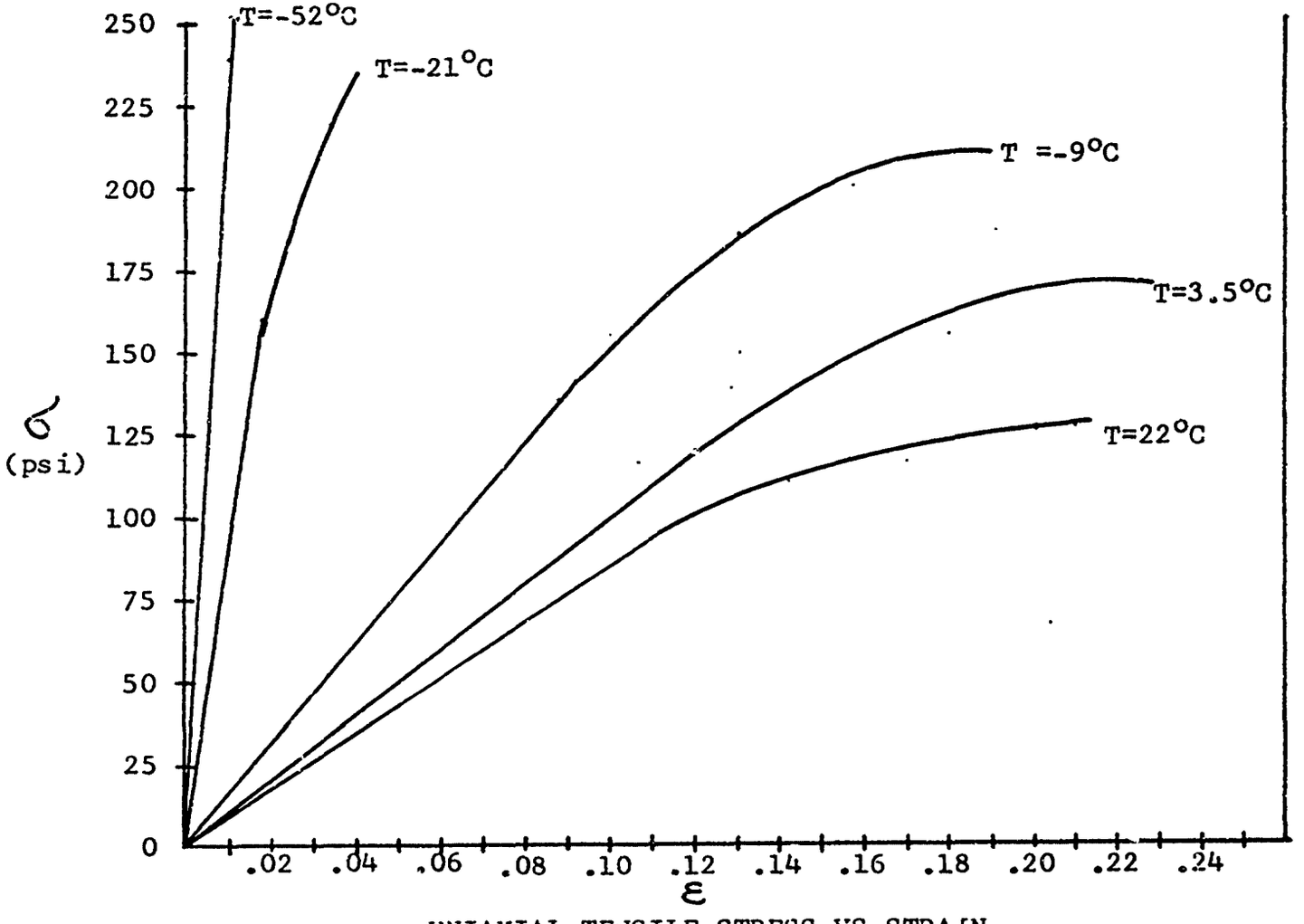

UNIAXIAL TENSILE STRESS VC STRAIN

Figure 10.

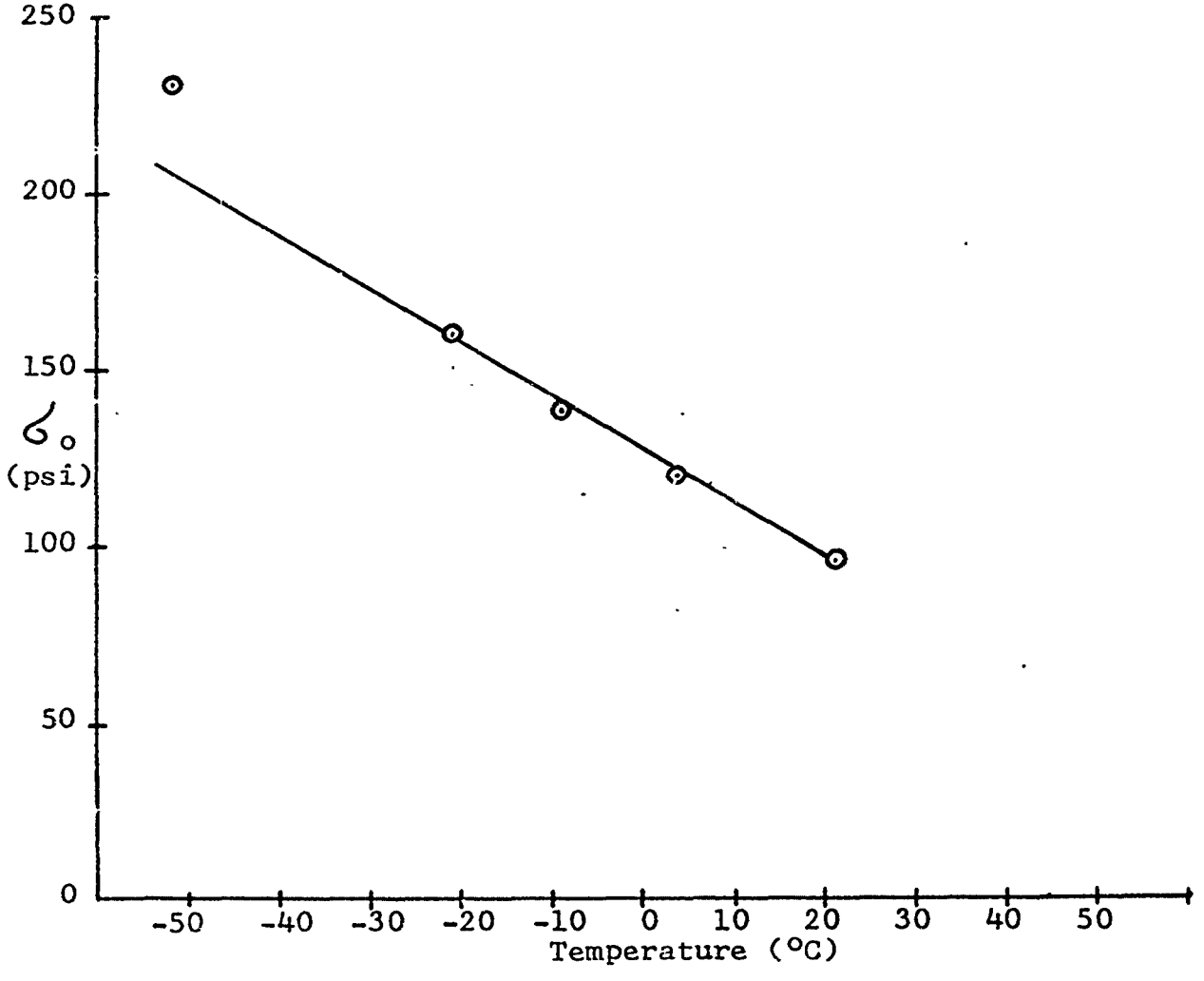

UNIAXIAL TENSILE YIELD STRESS VS TEMPERATURE

Figure 11.

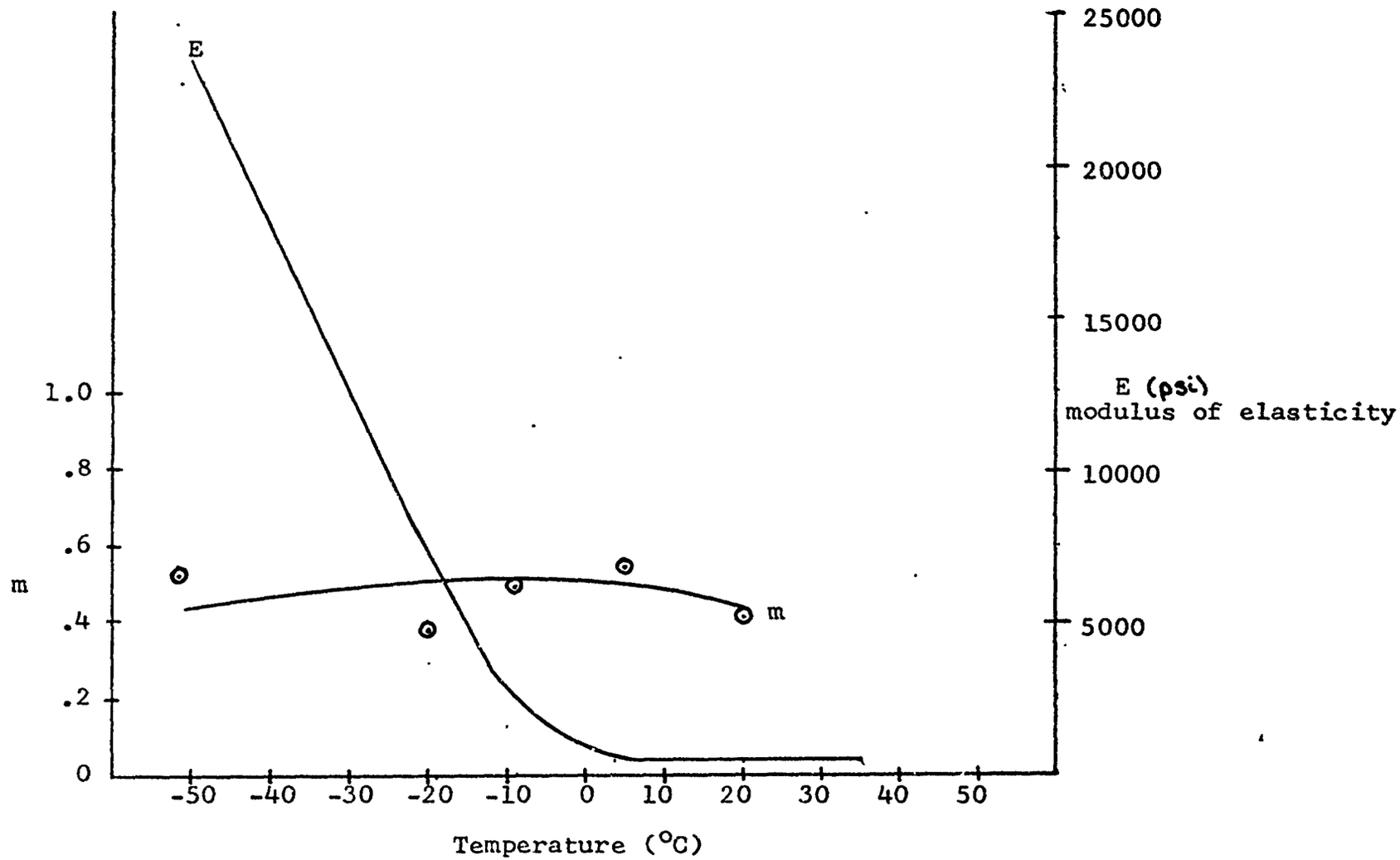

MODULUS AND LINEAR STRAIN HARDENING COEFFICIENT VS TEMPERATURE
Figure 12.

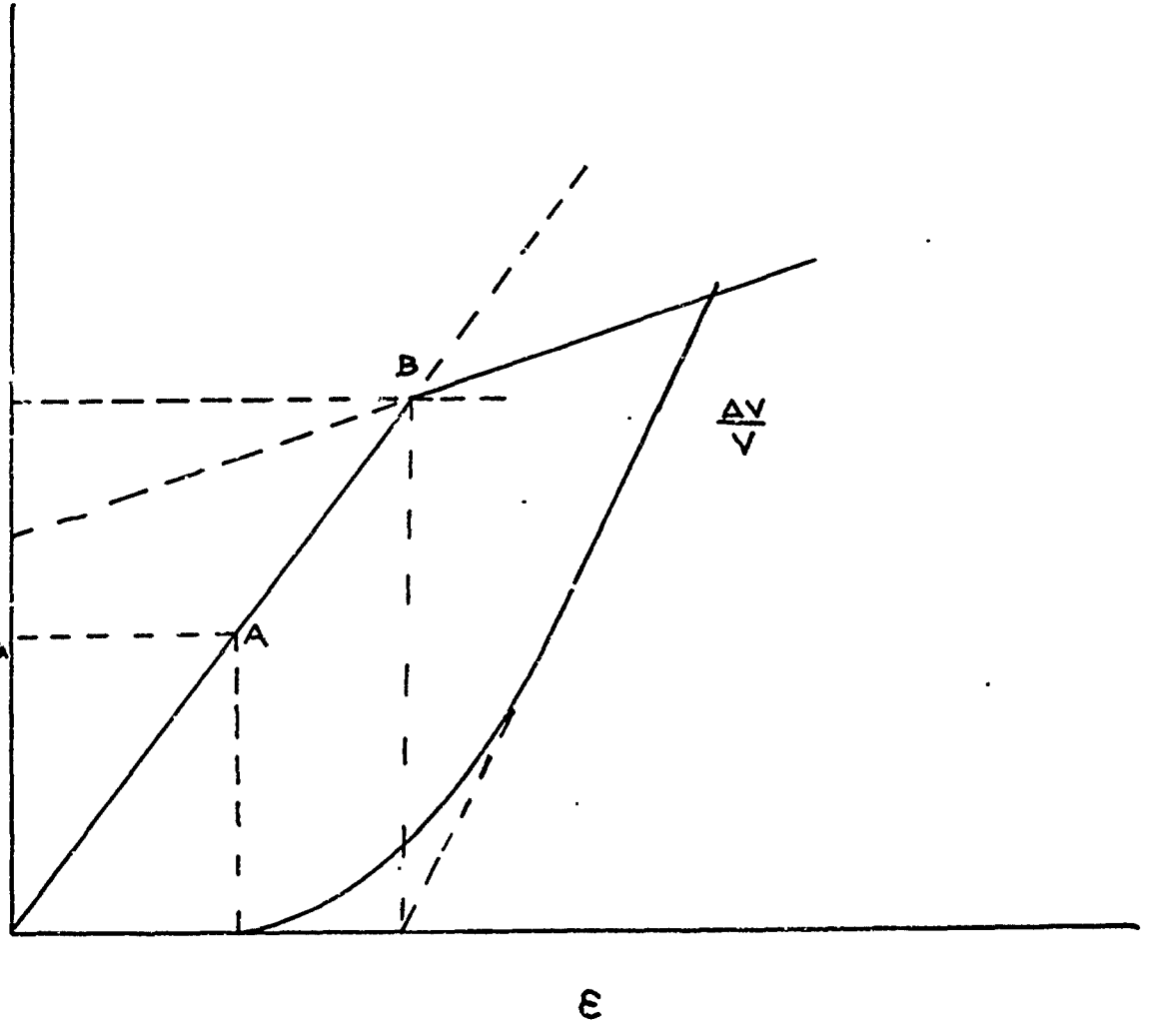

Calculated Uniaxial Tensile Yield Stress

Figure 13.

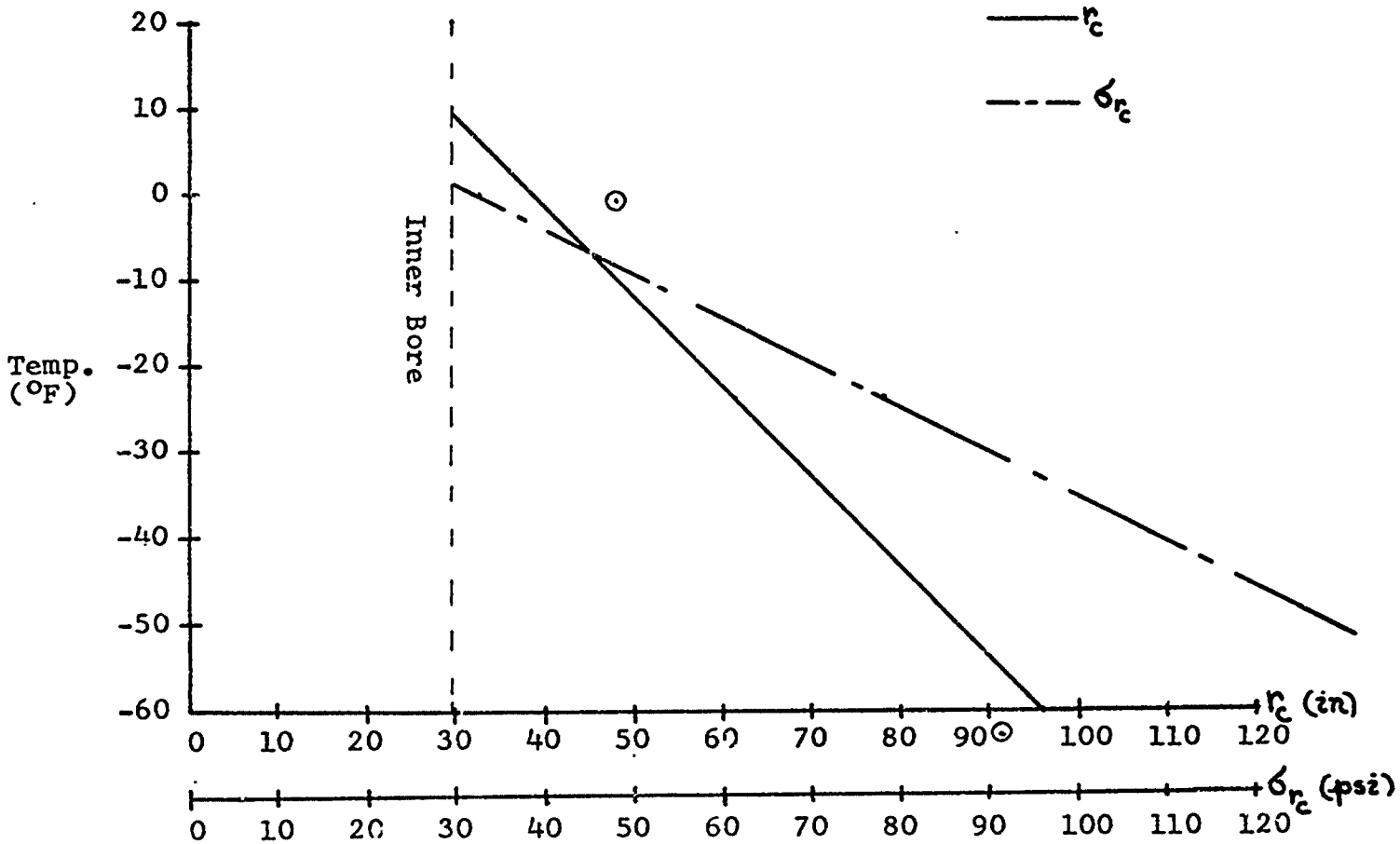

Critical Radius and Interface Pressure vs Temperature

Figure 14.

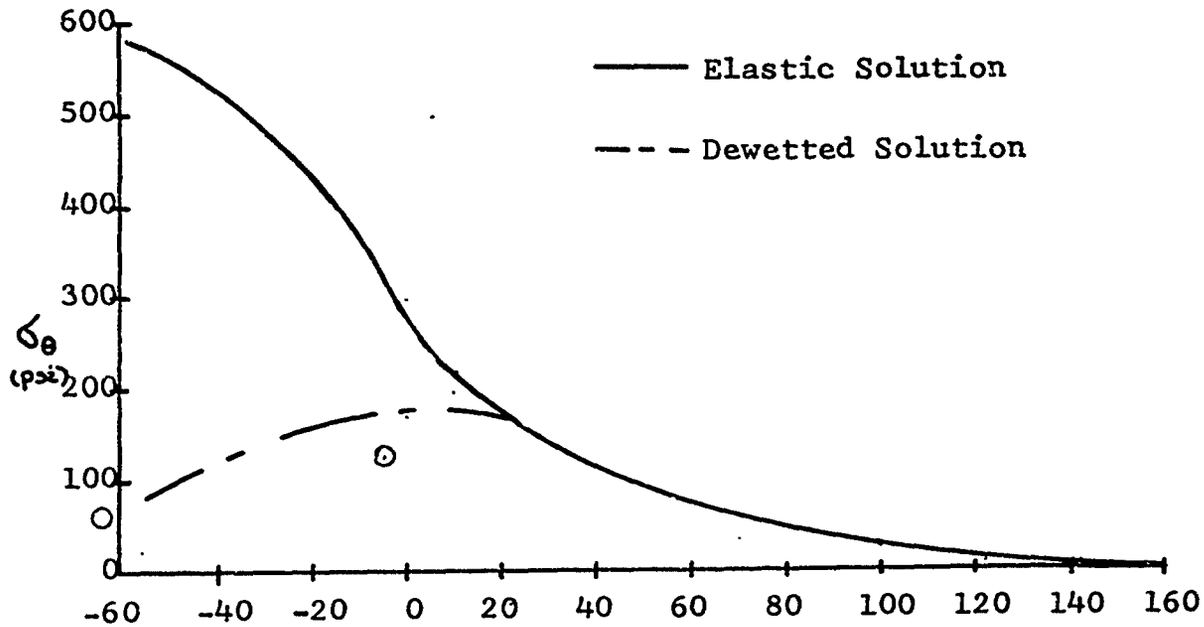

Inner Bore Tangential Stress vs Temperature

Figure 15.

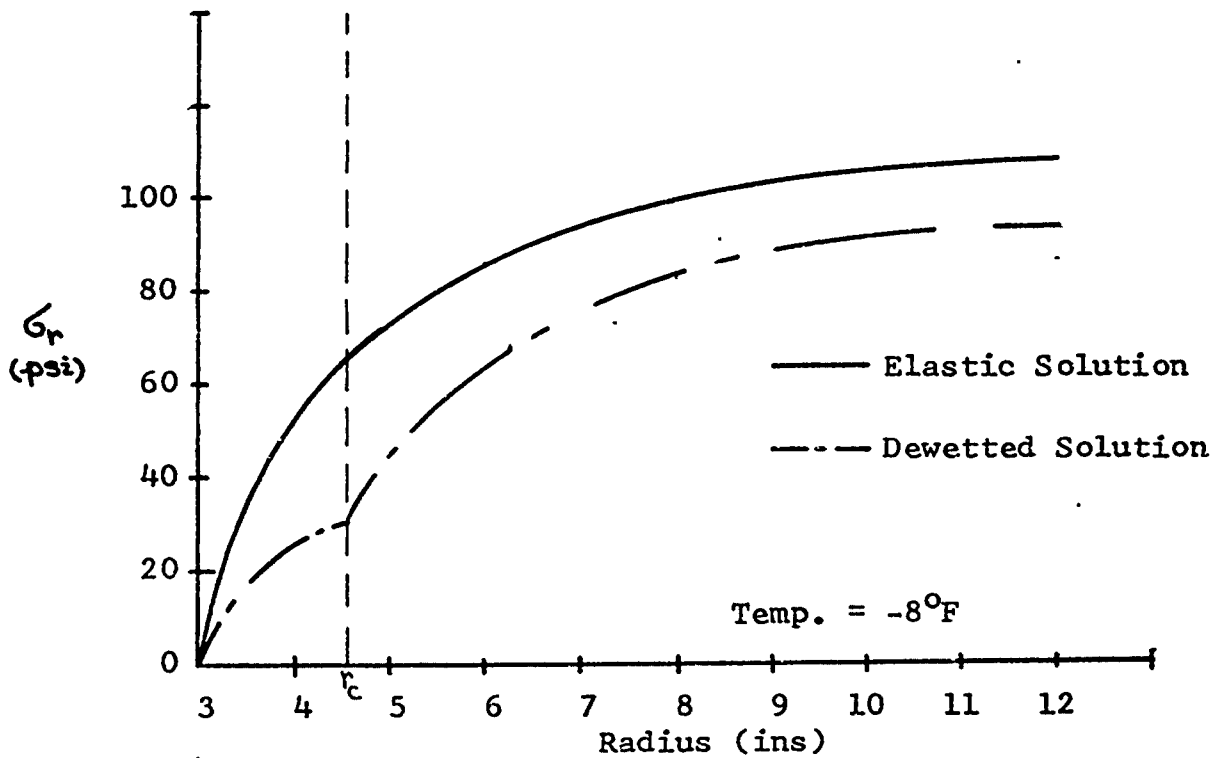

Radial Stress

Figure 16.

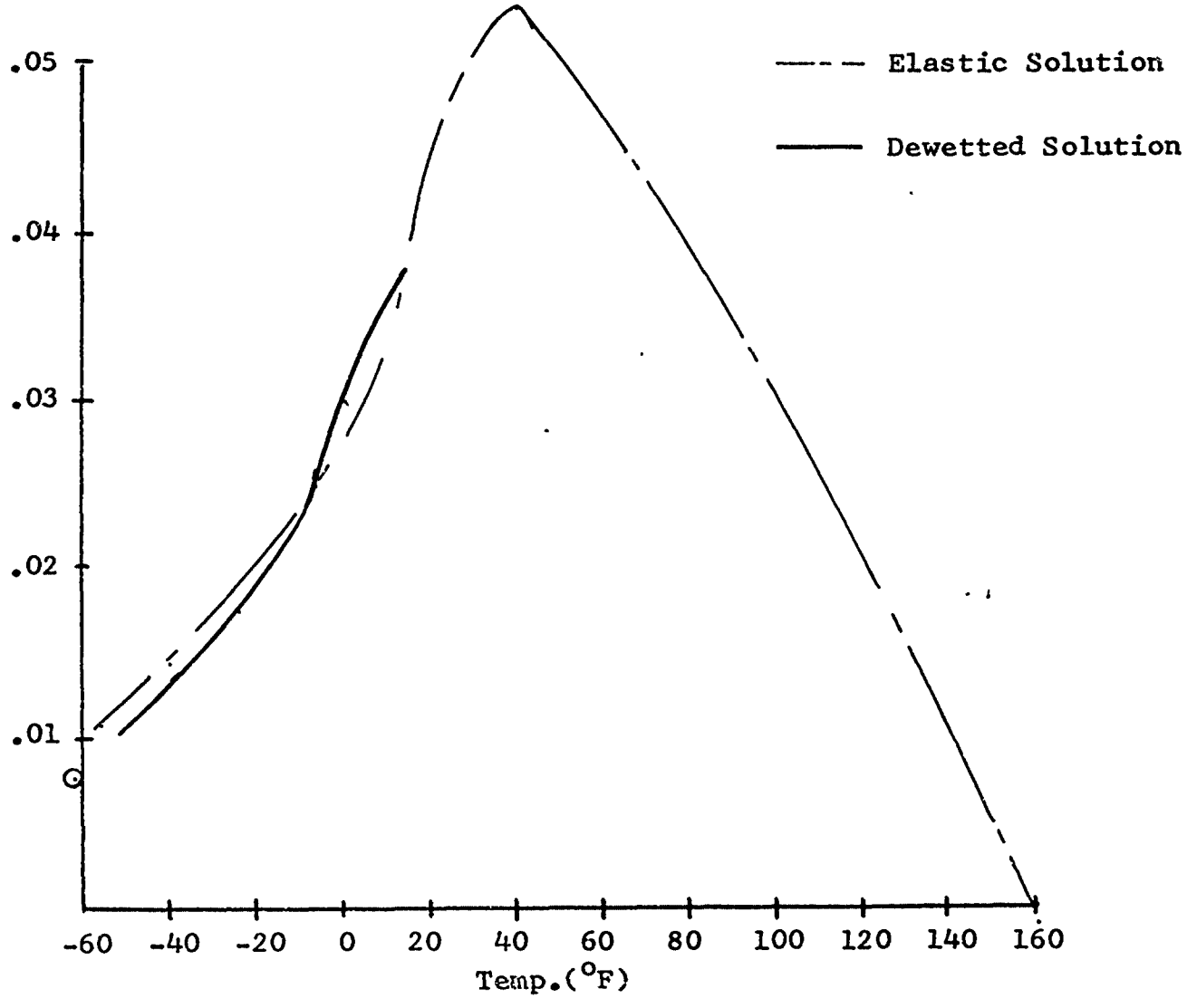

Tangential Strain vs Temperature

Figure 17.

APPENDIX A

ELASTIC SOLUTION

Williams, Blatz and Schapery (7) of the Guggenheim Aeronautical Laboratory (California Institute of Technology) analyzed solid propellant rocket motors of the same geometry under many different loading modes. Their basic assumptions were that

1. the propellant had material properties which were
   a. Isotropic
   b. Homogeneous
   d. Continuous
2. the strains were small.

Their solution to the thermally loaded, cylindrical, rocket motor, assuming a condition of plane strain, was:

$$\sigma_r = -\frac{b^2 p_c (1-a^2/r^2)}{(b^2-a^2)} + \frac{\alpha E (1-\frac{a^2}{r^2})}{(1-\nu)(b^2-a^2)}\int_a^b T r\,dr - \frac{\alpha E}{(1-\nu)r^2}\int_a^r T r\,dr$$

$$\sigma_\theta = -\frac{b^2 p_c (1+a^2/r^2)}{(b^2-a^2)} + \frac{\alpha E (1+\frac{a^2}{r^2})}{(1-\nu)(b^2-a^2)}\int_a^b T r\,dr + \frac{\alpha E}{(1-\nu)r^2}\int_a^r T r\,dr - \frac{\alpha E T}{(1-\nu)} \qquad \text{(A-1)}$$

$$\varepsilon_\theta = -\frac{(1+\nu)b^2 p_c\left((1-2\nu)b^2+\frac{a^2}{r^2}\right)}{E(b^2-a^2)} + \frac{(1+\nu)\alpha\left((1-2\nu)+\frac{a^2}{r^2}\right)}{(1-\nu)(b^2-a^2)}\int_a^b T r\,dr + \frac{(1+\nu)\alpha}{(1-\nu)r^2}\int_a^r T r\,dr$$

where

$$p_c = \frac{E\alpha\frac{2(1+\nu)}{(b^2-a^2)}\int_a^b T r\,dr - \alpha_c T(b)(1+\nu)E}{D}$$

$$D = \frac{(1+\nu)((1-2\nu)+a^2)}{b^2-a^2} + \frac{(1-\nu_c^2)bE}{hE_c}$$

And for the case of an internally pressurized rocket motor their solution was:

$$\sigma_r = \frac{a^2b^2(p_c-p_i)}{r^2(b^2-a^2)} + \frac{p_ia^2-p_cb^2}{b^2-a^2}$$

$$\sigma_\theta = -\frac{a^2b^2(p_c-p_i)}{r^2(b^2-a^2)} + \frac{p_ia^2-p_cb^2}{b^2-a^2} \qquad \text{(A-2)}$$

$$p_c = \frac{\frac{3}{2}\frac{a^2p_i}{b^2-a^2}}{D}$$

where p_i = internal pressure

In considering the effects of dewetting, the inner boundary condition changed. The inner radius of the elastic region was the same as the critical radius, i.e., it was equal to the radius of the dewetting surface. As the dewetting surface moved outward, the inner radius of the elastic zone also increased; furthermore the inner boundary was no longer stress free. From continuity of the radial stress across the dewetting surface, it was seen that the inner boundary now had a stress equal to σ_{r_c} induced upon it. This elastic solution was obtained by combining A-1 and A-2, and setting p_i equal to σ_{r_c}, and the inner radius, a, equal to the critical radius, r_c

$$\sigma_r = \frac{\sigma_{r_c}r_c^2\left(r^2-b^2+\frac{3b^2(r_c^2+r^2)}{2(b^2-r_c^2)D}\right) - \frac{3b^2(r_c^2+r^2)}{2D}ET(\alpha-\alpha_c)}{r^2(b^2-r_c^2)}$$

$$\sigma_\theta = \frac{\sigma_{r_c}r_c^2\left(r^2+b^2-\frac{3b^2(r_c^2+r^2)}{2(b^2-r_c^2)D}\right) - \frac{3b^2(r_c^2+r^2)}{2D}ET(\alpha-\alpha_c)}{r^2(b^2-r_c^2)} \qquad \text{(A-3)}$$

$$p_c = \frac{\frac{3}{2}ET(\alpha-\alpha_c)+\frac{3}{2}\frac{r_c^2\sigma_{r_c}}{b^2-r_c^2}}{D} \qquad D = \frac{3}{2}\frac{r_c^2}{(b^2-r_c^2)} + \frac{(1-\nu_c^2)bE}{hE_c}$$

LIST OF REFERENCES

1. B. Budiansky, "A Reassessment of Deformation Theories of Plasticity," Journal of Applied Mechanics, Vol. 26, 1959, pp. 259-264.

2. R. Hill, E. H. Lee, S. J. Tupper, "The Theory of Combined Plastic and Elastic Deformation with Particular Reference to a Thick Tube Under Internal Pressure," Proceedings of the Royal Society of London, Series A, Vol. 191, 1947, p. 278.

3. G. H. Lindsey, "Studies Pertaining to Solid Propellant Fracture," NPS-57Li72011A, Naval Postgraduate School, 1972.

4. G. H. Lindsey, and J. F. Wood, "An Isotropic Theory for Dewettable Solids," NPS-57Li71011A Naval Postgraduate School, 1971.

5. A. Mendelson, "Plasticity: Theory and Application," MacMillan and Company, 1970.

6. M. C. Steele, "Partially Plastic Thick-Walled Cylinder Theory," Journal of Applied Mechanics, Vol. 19, 1957, pp. 133-141.

7. M. L. Williams, P. J. Blatz, and R. A. Schapery, "Fundamental Studies Relating to Systems Analysis of Solid Propellants," Guggenheim Aeronautical Laboratory, California Institute of Technology, Pasadena, California, 1961.

8. J. E. Wood, PHD Thesis in preparation, Aeronqutics Department, Naval Postgraduate School, 1972.